



## Density functional theory studies on the oleic acid thermal oxidation into volatile compounds

Lin Xiao<sup>a,d,1</sup>, Shang Wang<sup>c,1</sup>, Yi Wang<sup>c</sup>, Binchen Wang<sup>a,b</sup>, Chaofan Ji<sup>a,b</sup>, Xinping Lin<sup>a,b</sup>, Huipeng Liang<sup>a,b</sup>, Sufang Zhang<sup>a,b</sup>, Xianbing Xu<sup>a,b</sup>, Liang Dong<sup>a,b,\*</sup>

<sup>a</sup> School of Food Science and Technology, Dalian Polytechnic University, Dalian 116034, Liaoning, China

<sup>b</sup> National Engineering Research Center of Seafood, Dalian 116034, Liaoning, China

<sup>c</sup> School of Biotechnology, Dalian Polytechnic University, Dalian 116034, Liaoning, China

<sup>d</sup> China Resources Snow Beer, Beijing 100000, Beijing, China

### ARTICLE INFO

#### Keywords:

Oleic acid oxidation  
Flavor  
Density functional theory  
GC-MS  
Quantum chemistry

### ABSTRACT

Oleic acid oxidation is one of the main sources of food flavor compounds. Volatile profiling was investigated using thermal desorption cryo-trapping combined with gas chromatography–mass spectrometry to analyze the volatile composition of oleic acid oxidation. A total of 43 volatile compounds, including aldehydes (11), ketones (2), alcohols (5), furans (2), acids (8), ester (12) and alkane (3) were identified from oleic acid during heating. Then, density functional theory (DFT) was applied to analyze the oxidative mechanism of oleic acid during heating. A total of 30 reactions were obtained and grouped into the peroxide (ROOH), alkoxy radical (RO●), and peroxide radical (ROO●) pathways. The structures of intermediates, transition states (TS), and products in each reaction were also determined. Results show that the branch chemical reactions were the key reactions in different reaction pathway. Moreover, the reaction priority of the thermal oxidation reaction of oleic acid was the peroxide radical mechanism > the peroxide mechanism > the alkoxy radical mechanism.

### Introduction

Lipid oxidation is one of the major sources of food flavor compounds (Frankel, 1980; Frankel, 1984). Oleic acid is the main component of lipids, and aldehydes, ketones, alcohols, acids, and furans resulting from its oxidative decomposition is the major substances of food flavor (Xie, Xu, Xu, Yao, Zhu, Li, et al., 2022; Bao, Du, Xu, Wang, Wang, Xiao, et al., 2022). The oxidation process of oleic acid is considered as a typical free radical oxidation reaction with three steps: initiation, propagation, and termination (Zhao, Yang, Shi, Pan, Zhang, Zhang, et al., 2011).

As shown in Fig. 1A, during food heating, high temperature acts as an initiating factor for the free radical reaction (Li, Luo, Wang, & Cen, 2020; Otero, Ramos, de Elvira, & Sanz, 2007). The main step of propagation starts with the formation of peroxy radicals (ROO●). The radicals then take over the hydrogen atoms to form peroxides. During heating, the peroxides are unstable, and the —O—O— bond is easily broken to form alkoxy radicals. Alkoxy radicals undergo further  $\beta$ -unimolecular cleavage, which generates short-chain volatile compounds. The

decomposition of hydroperoxides is an important propagation link in the radical chain (Turovskyj, Raksha, Opeida, Turovska, & Zaikov, 2007; Endo, Sakamoto, Kajii, & Enami, 2022). The final radicals undergo bimolecular reactions to form triacylglycerol polymers, which leading to the termination of the radical chain reaction (Zhao, Yang, Shi, Pan, Zhang, Zhang, et al., 2011).

Theoretical chemistry, as a theoretical and computational approach to study chemical reactions, has been widely used in studying the chemical reaction mechanism in recent years (Raos, 2021). Unlike experimental chemistry, theoretical chemistry could delve into the microscopic nature of reactions, and its results are not influenced by environmental factors (Friedrich, B., 2016). The density functional theory (DFT) in theoretical chemistry could determine the structures and thermodynamic parameters of different reactants and products in chemical reactions. Meanwhile, the active sites of functional groups and the activation energy of reactions could also be determined (Kvasyuk, Sysa, Al Saud, Shahab, Sheikhi, Kaviani, et al., 2023; Elqahani, Aman, Mehmood, Ali, Hussanan, Ahmad, et al., 2022). Food thermal processing

\* Corresponding author at: School of Food Science and Technology, National Engineering Research Center of Seafood, Dalian Polytechnic University, Qinggongyuan Road No.1, Dalian 116034, China.

E-mail address: [dongliang@dpu.edu.cn](mailto:dongliang@dpu.edu.cn) (L. Dong).

<sup>1</sup> Lin Xiao and Shang Wang contributed equally to this study.

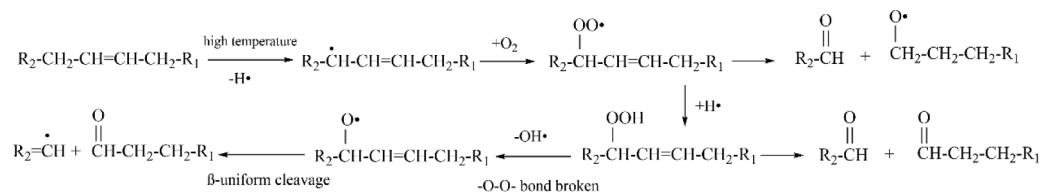
<https://doi.org/10.1016/j.fochx.2023.100737>

Received 23 February 2023; Received in revised form 27 May 2023; Accepted 1 June 2023

Available online 7 June 2023

2590-1575/© 2023 The Author(s). Published by Elsevier Ltd. This is an open access article under the CC BY-NC-ND license (<http://creativecommons.org/licenses/by-nc-nd/4.0/>).

A



B

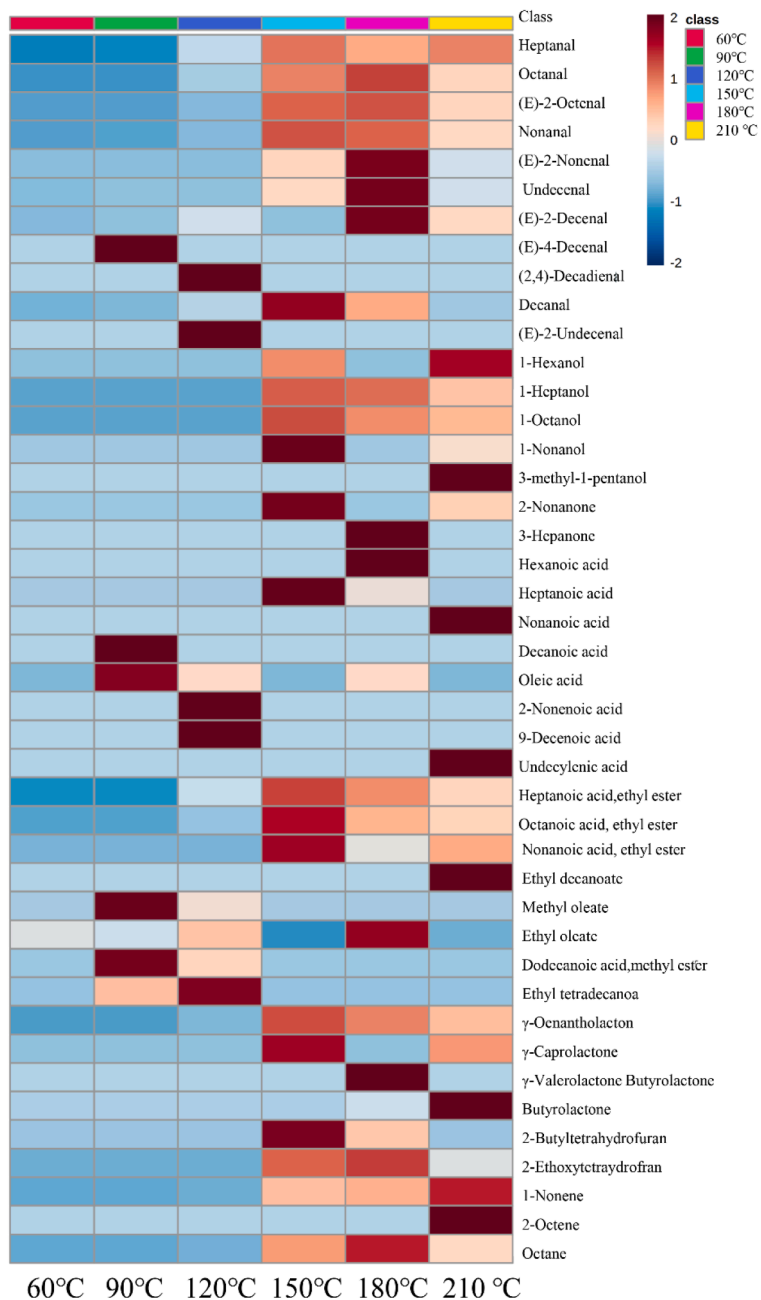


**Fig. 1.** Free radical reaction mechanism and heatmaps of volatile compounds from oleic acid oxidation. (A): Diagram of free radical reaction mechanism. (B): Heatmaps of volatile compounds from oleic acid oxidation at different heating temperature.

**Table 1**  
Volatile compounds from oleic acid oxidation during heating.

No	compound	RI	LRI	Method of identification	Concentration ( µg/mg)					
					60°C	90°C	120°C	150°C	180°C	210°C
<b>Aldehydes</b>										
1	Heptanal	927	900 (Huang et al., 2019)	RI,MS,STD	nd	0.07 ± 0.01 <sup>d</sup>	1.16 ± 0.04 <sup>c</sup>	2.81 ± 0.29 <sup>a</sup>	2.39 ± 0.15 <sup>b</sup>	2.80 ± 0.20 <sup>a</sup>
2	Octanal	1003	1008 (Wang et al., 2014)	RI,MS,STD	nd	nd	3.06 ± 0.23 <sup>c</sup>	10.48 ± 0.21 <sup>a</sup>	10.90 ± 0.21 <sup>a</sup>	10.04 ± 0.19 <sup>b</sup>
3	(E)-2-Octenal	1059	1059 (Liu, Wang, Tamogami, Chen, & Zhang, 2021)	RI,MS,STD	nd	nd	0.35 ± 0.04 <sup>d</sup>	2.30 ± 0.14 <sup>b</sup>	3.45 ± 0.26 <sup>a</sup>	3.56 ± 0.18 <sup>c</sup>
4	Nonanal	1103	1105 (Huang et al., 2018)	RI,MS,STD	0.11 ± 0.01 <sup>e</sup>	0.30 ± 0.01 <sup>e</sup>	2.84 ± 0.26 <sup>d</sup>	25.38 ± 0.44 <sup>a</sup>	23.93 ± 0.23 <sup>b</sup>	10.60 ± 1.00 <sup>c</sup>
5	(E)-2-Nonenal	1162	1161 (Zhou, Liu, Liu, & Song, 2019)	RI,MS,STD	nd	nd	0.80 ± 0.02 <sup>b</sup>	0.39 ± 0.03 <sup>c</sup>	0.19 ± 0.00 <sup>d</sup>	0.99 ± 0.18 <sup>a</sup>
6	Decanal	1206	1205 (Huang et al., 2018)	RI,MS,STD	nd	0.06 ± 0.01 <sup>e</sup>	0.42 ± 0.02 <sup>d</sup>	2.57 ± 0.07 <sup>a</sup>	1.47 ± 0.02 <sup>b</sup>	0.63 ± 0.04 <sup>c</sup>
7	(E)-2-Decenal	1263	1263 (Xiao et al., 2020)	RI,MS,STD	nd	2.74 ± 0.27 <sup>d</sup>	18.29 ± 0.30 <sup>c</sup>	2.79 ± 0.30 <sup>d</sup>	90.82 ± 0.26 <sup>a</sup>	33.58 ± 0.29 <sup>b</sup>
8	(E)-4-Decenal	1190	1191 (Huang et al., 2018)	RI,MS,STD	nd	0.09 ± 0.01 <sup>a</sup>	nd	nd	nd	nd
9	(2,4)-Decadienal	1371	1317 (Liu, Wang, Tamogami, Chen, & Zhang, 2021; Zhou, Liu, Liu, & Song, 2019)	RI,MS,STD	nd	nd	0.38 ± 0.02 <sup>a</sup>	nd	nd	nd
10	Undecanal	1300	1309 (Wang et al., 2014)	RI,MS,STD	0.33 ± 0.07 <sup>e</sup>	3.04 ± 0.23 <sup>d</sup>	nd	37.82 ± 2.18 <sup>b</sup>	104.16 ± 2.35 <sup>a</sup>	19.70 ± 0.21 <sup>c</sup>
11	(E)-2-Undecenal	1367	1360 (Liu et al., 2020)	RI,MS,STD	nd	nd	32.24 ± 0.51 <sup>a</sup>	nd	nd	nd
<b>Alcohols</b>										
12	3-methyl-1-Pentanol	838	838 (Xiao et al., 2020)	RI,MS,STD	nd	nd	nd	nd	nd	0.05 ± 0.01 <sup>a</sup>
13	1-Hexanol	868	886 (Cheng et al., 2015)	RI,MS,STD	nd	nd	nd	0.17 ± 0.00 <sup>b</sup>	nd	0.23 ± 0.01 <sup>a</sup>
14	1-Heptanol	970	970 (Xiao et al., 2020)	RI,MS,STD	nd	nd	nd	3.07 ± 0.29 <sup>a</sup>	2.86 ± 0.16 <sup>a</sup>	1.94 ± 0.11 <sup>b</sup>
15	1-Octanol	1071	1088 (Cheng et al., 2015)	RI,MS,STD	nd	nd	nd	6.09 ± 0.02 <sup>a</sup>	5.29 ± 0.07 <sup>b</sup>	4.66 ± 0.28 <sup>c</sup>
16	1-Nonanol	1173	1190 (Cheng et al., 2015)	RI,MS,STD	nd	nd	nd	0.36 ± 0.08 <sup>a</sup>	nd	0.10 ± 0.01 <sup>b</sup>
<b>Acid</b>										
17	Hexanoic acid	990	1002 (Cheng et al., 2015)	RI,MS,STD	nd	nd	nd	nd	0.44 ± 0.00 <sup>a</sup>	nd
18	Heptanoic acid	1078	1078 (Benkhoud, Rabet, Gara Ali, Mezni, & Hosni, 2022)	RI,MS,STD	nd	nd	nd	3.60 ± 0.22 <sup>a</sup>	0.76 ± 0.06 <sup>b</sup>	nd
19	Nonanoic acid	1273	1273 (Matheis & Granvogel, 2019; Zhou, Liu, Liu, & Song, 2019)	RI,MS,STD	nd	nd	nd	nd	nd	2.35 ± 0.28 <sup>a</sup>
20	Decanoic acid	1373	1370 (Cheng et al., 2015)	RI,MS,STD	nd	0.20 ± 0.01 <sup>a</sup>	nd	nd	nd	nd
21	2-Nonenoic acid	1321	1325 (Cheng et al., 2015)	RI,MS,STD	nd	nd	0.16 ± 0.00 <sup>a</sup>	nd	nd	nd
22	9-Decenoic acid	1374	1389 (Benkhoud et al., 2022)	RI,MS,STD	nd	nd	0.32 ± 0.02 <sup>a</sup>	nd	nd	nd
23	Undecylenic acid	1484	1478 (Benkhoud et al., 2022)	RI,MS	nd	nd	nd	nd	nd	0.73 ± 0.03 <sup>a</sup>
24	Oleic acid	2141	2156 (Benkhoud et al., 2022)	RI,MS,STD	nd	0.26 ± 0.00 <sup>a</sup>	0.10 ± 0.01 <sup>b</sup>	nd	0.10 ± 0.00 <sup>b</sup>	nd
<b>Ketone</b>										
25	2-Heptanone	887	891 (Wang et al., 2020)	RI,MS,STD	nd	nd	nd	nd	0.03 ± 0.00 <sup>a</sup>	nd
26	2-Nonanone	1092	1096 (Wang et al., 2014)	RI,MS,STD	nd	nd	nd	0.56 ± 0.03 <sup>a</sup>	nd	0.22 ± 0.03 <sup>b</sup>
<b>Ester</b>										
27	Butyrolactone	915	915 (Xiao et al., 2020)	RI,MS	nd	nd	nd	nd	0.08 ± 0.00 <sup>b</sup>	0.79 ± 0.09 <sup>a</sup>
28	γ-Valerolactone	943	946 (Cheng et al., 2015)	RI,MS	nd	nd	nd	nd	0.21 ± 0.00 <sup>a</sup>	nd
29	γ-Oenantholacton	1078	1093 (Wang et al., 2014)	RI,MS	nd	nd	0.13 ± 0.01 <sup>d</sup>	1.18 ± 0.03 <sup>b</sup>	0.96 ± 0.06 <sup>b</sup>	0.80 ± 0.06 <sup>c</sup>
30	Heptanoic acid,ethyl ester	1097	1097 (Wang et al., 2020)	RI,MS	nd	nd	0.41 ± 0.01 <sup>d</sup>	1.25 ± 0.06 <sup>a</sup>	1.05 ± 0.04 <sup>b</sup>	0.75 ± 0.07 <sup>c</sup>
31	Octanoic acid,ethyl ester	1196	1196 (Wang et al., 2020)	RI,MS	nd	nd	0.52 ± 0.04 <sup>d</sup>	3.71 ± 0.27 <sup>a</sup>	2.16 ± 0.05 <sup>b</sup>	1.87 ± 0.06 <sup>c</sup>
32	Nonanoic acid, ethyl ester	1296	1296 (Wang et al., 2020)	RI,MS	nd	nd	nd	5.30 ± 0.17 <sup>a</sup>	1.64 ± 0.04 <sup>c</sup>	3.07 ± 0.25 <sup>b</sup>
33	Ethyl decanoate	1396	1390 (Huang et al., 2019)	RI,MS	nd	nd	nd	nd	nd	0.10 ± 0.02 <sup>a</sup>

(continued on next page)

Table 1 (continued)

No	compound	RI	LRI	Method of identification	Concentration ( µg/mg)					
					60°C	90°C	120°C	150°C	180°C	210°C
34	Dodecanoic acid, methyl ester	1526	1530 (Cheng et al., 2015)	RI,MS	nd	0.12 ± 0.00 <sup>a</sup>	0.04 ± 0.01 <sup>b</sup>	nd	nd	nd
35	Ethyl tetradecanoate	1794	1778 (Benkhoud et al., 2022)	RI,MS	nd	0.01 ± 0.00 <sup>ab</sup>	0.03 ± 0.00 <sup>a</sup>	nd	nd	nd
36	γ-Caprolactone	1860	1886 (Wang et al., 2014)	RI,MS	nd	nd	nd	0.80 ± 0.03 <sup>a</sup>	nd	0.65 ± 0.02 <sup>b</sup>
37	Methyl oleate	2091	2100 (Cheng et al., 2015)	RI,MS	nd	1.41 ± 0.03 <sup>a</sup>	0.13 ± 0.03 <sup>b</sup>	nd	nd	nd
38	Ethyl Oleate	2173	2154 (Cheng et al., 2015)	RI,MS	nd	0.78 ± 0.08 <sup>c</sup>	1.22 ± 0.04 <sup>b</sup>	nd	2.60 ± 0.15 <sup>a</sup>	0.27 ± 0.04 <sup>d</sup>
<b>Furan</b>										
39	2-Ethoxytetrahydrofuran	943	930 (Wang et al., 2014)	RI,MS	nd	nd	nd	4.48 ± 0.15 <sup>b</sup>	5.03 ± 0.24 <sup>a</sup>	1.88 ± 0.07 <sup>c</sup>
40	2-butyltetrahydrofuran	1004	1000 (Huang et al., 2019)	RI,MS	nd	nd	nd	0.22 ± 0.00 <sup>a</sup>	0.09 ± 0.00 <sup>b</sup>	nd
<b>Hydrocarbon</b>										
41	2-Octene	810	817 (Huang et al., 2019)	RI,MS,STD	nd	nd	nd	nd	nd	0.23 ± 0.01 <sup>a</sup>
42	Octane	800	800 (Huang et al., 2019)	RI,MS,STD	nd	nd	0.43 ± 0.00 <sup>d</sup>	7.52 ± 0.45 <sup>b</sup>	10.90 ± 0.41 <sup>a</sup>	5.04 ± 0.47 <sup>c</sup>
43	1-Nonene	889	894 (Huang et al., 2019)	RI,MS,STD	nd	nd	0.08 ± 0.01 <sup>c</sup>	1.40 ± 0.14 <sup>b</sup>	1.52 ± 0.15 <sup>b</sup>	2.44 ± 0.23 <sup>a</sup>

Nd = Compound not detected in the sample. MS = Identification by MS spectra, RI = Kovat's retention indexes, STD = Comparison with a standard compound; Concentration is the mean ± standard error of three replicates; "a,b, c, d" indicates a significant difference ( $p < 0.05$ ).

is very complex, with many chemical reactions occurred. Therefore, application of DFT in food thermal processing could effectively explore chemical reactions occurred in this process to deeply reveal the food flavor forming mechanism.

In this study, the mechanism of volatile flavor formation during thermal oxidation of oleic acid is discussed in detail by applying DFT with experimental data. Volatile profiling is investigated using thermal desorption cryo-trapping combined with gas chromatography–mass spectrometry. Then, DFT is applied to study the mechanism of volatile flavor production from the thermal oxidation of oleic acid.

## Materials and methods

### Chemicals

Standard chemicals: Heptanal (≥98.5%), Octanal (≥99.5%), (E)-2-Octenal (≥97.5%), Nonanal (≥95%), (E)-2-Nonenal (≥99.5%), Decanal (≥99.9%), (E)-2-Decenal (≥95%), (E)-4-Decenal (≥97%), (2,4)-Decadienal (≥90%), Undecanal (≥95%), (E)-2-Undecenal (≥90%), 3-methyl-1-Pentanol (≥95%), 1-Hexanol (≥95%), 1-Heptanol (≥99%), 1-Octanol (≥98%), Nonanol (≥95%), Hexanoic acid (≥95%), Heptanoic acid (≥97%), Nonanoic acid (≥99%), Decanoic acid (≥99%), 2-Nonenoic acid (≥80%), 9-Decenoic acid (≥95%), 3-Heptanone (≥90%), 2-Nonanone (≥99%), 2-Octene (≥95%), Octane (≥97%), 1-Nonene (≥99%), oleic acid and C4–C20 *n*-alkanes (analytical grade) were purchased from Sigma-Aldrich (Shanghai, China).

### Extraction and collection of volatile compounds from oleic acid during heating by using a thermal desorption cryo-trapping system

Simulative heating was performed using a qualified Micro-chamber/Thermal Extractor (M-CTE250 Markes International, UK). The M-CTE250 is a quality control tool for screening volatile and semi-volatile organic compounds coming out of organic materials. The chambers of the M-CTE, *o*-rings and sample holders were firstly rinsed with ethanol and cyclohexane. Then, a 20 mL volume glassware was placed in the sample holder, 20 µL of oleic acid and 10 µL diluted cyclohexanone (0.5 mg/mL) used as the quantitative internal standard were added directly into the glassware. Afterwards, the lid of the sample holder was quickly closed. Three sample holders were used simultaneously for parallel

experiments (one sample per chamber) and were heated at 60 °C, 90 °C, 120 °C, 150 °C, 180 °C and 210 °C for 30 min. Finally, the air valve was opened with a flow rate of 100 mL/min for 30 min per temperature to extract volatile and semi-volatile compounds from the sample. These molecules were trapped in 250 mg Tenax TA adsorbent tubes (60–80 mesh). After the molecules were trapped, volatile compounds were thermally desorbed from sorbent tubes using an automated thermal desorber (TD100-xr Markes International) at 280 °C for 5 min, cryo-focussed on a cold trap at 10 °C and desorbed from the cold trap onto the gas chromatography–mass spectrometry column by flash heating at 280 °C for 3 min with a flow path temperature of 200 °C.

### GC–MS analysis

An Agilent 7890/5975C GC–MS (Santa Clara, CA, USA) system equipped with HP-5 ms column (30 m × 0.25 mm i.d., 0.25 µm film thickness; J&W Scientific) was used to analyze volatile compounds that desorbed from the cold trap. The carrier gas was helium with a linear velocity of 1 mL/min. GC injector was operated in the splitless mode. Desorption time was 5 min in the injection port at 250 °C. The temperature was programmed to be hold at 35 °C for 3 min and increased to 280 °C at a rate of 5 °C/min. The mass selective detector was operated in the electron impact ionization mode at 70 eV, in the scan range  $m/z$  40–400. The interface temperature was 230 °C. The retention time of each volatile identified was converted to the Kovats retention indices (RI), which were calculated by using C4–C20 *n*-alkanes (Sigma, Co.) as references (Chenga, Chena, Li, et al., 2015). The volatile compounds were tentatively identified by matching the mass spectra with the spectra of the reference compounds in both the Wiley mass spectra (MS) library (8th edn) and the NIST/EPA/NIH MS library (2014 version) and verified on the basis of mass spectra obtained from the literature and comparison of Kovats retention indices with those reported in the literature (Chen, Li, Yu, Wang, Blank, Zhang, Liu, et al., 2023). Finally, identification accuracy was determined by separating relevant standard compounds through GC–MS analysis under the same conditions (Chai, Li, Zhang, Yang, Liu, Xu, et al., 2019).

### Computational methods

All calculations in this study were done on the Gaussian16 software

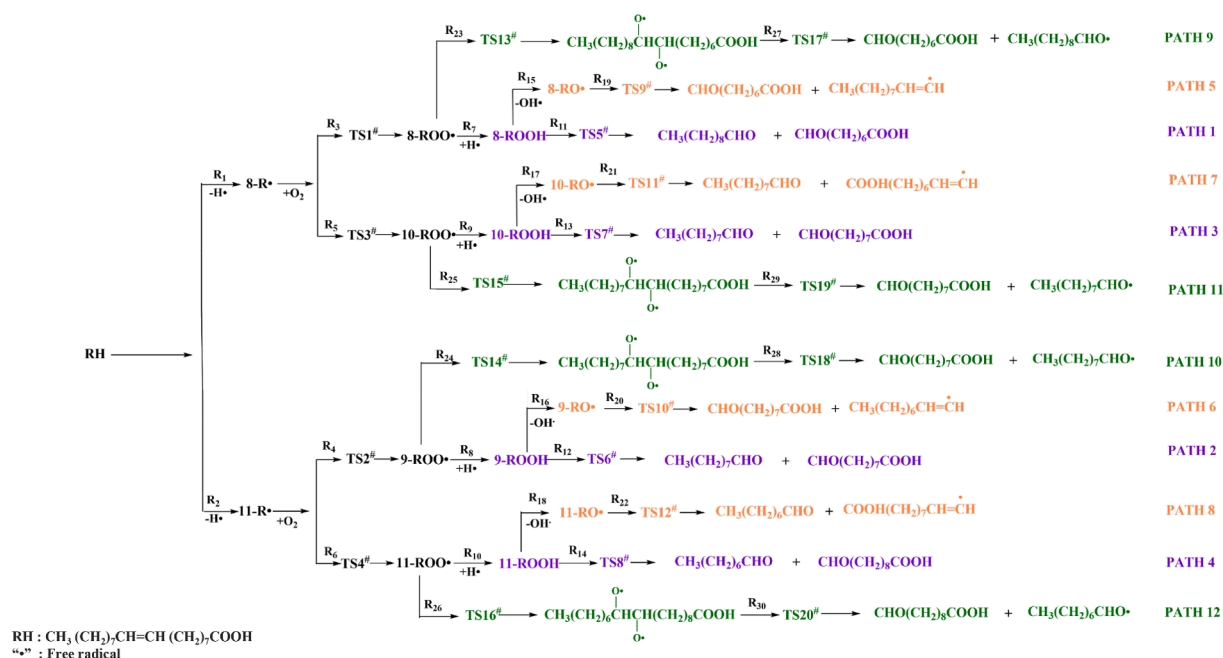


**Fig. 2.** Total reaction diagram of oleic acid thermal oxidation process based on the DFT calculation results. Purple: peroxide (ROOH) pathway; Orange: alkoxy radical (RO•) pathway; Green: peroxide radical (ROO•) pathway. (For interpretation of the references to color in this figure legend, the reader is referred to the web version of this article.)

package (Müller, Shabani, Wagenpfeil, & Vogt, 2021; Shabani et al., 2020). Geometry optimizations for the molecular ions, intermediates, and fragments were carried out at the unrestricted B3LYP (UB3LYP) density functional levels of theory using the 6-311G (d, p) basis set (Elroby, Banaser, Aziz, Jedidi, Hassan, & Osman, 2022; Pedersen & Mikkelsen, 2022). Transition state (TS) geometries connecting the stable structures were searched at the same level. All the TS geometries found were checked by calculating the intrinsic reaction coordinates (IRC). The calculation of the point singlet energy was performed on the basis set of the high level Def2TZVP and combined with the results of the frequency calculations by using the Shermo 2.0.8 program for the Gibbs free energy to obtain an accurate reaction potential energy surface (González, Giménez, & Bofill, 2002; Raghavachari, Trucks, Pople, & Head-Gordon, 1989). The energy closest to the reaction saddle point was found as the Gibbs free energy required for the completion of the reaction. Reaction rate constants were determined by the identified reaction potential energy surface, relevant properties of the reactants, and transition states. The TSTcalculator could be used to calculate reaction rate constants (Ryu, Park, Kim, Park, Kim, & Baik, 2018; Mahmoud, Shiroudi, Abdel-Rahman, Shibl, Abdel-Azeim, & El-Nahas, 2021).

#### Calculation of molecular orbitals

The Chemcraft molecular analysis program was used to obtain the charge density of each atom in the molecule (Wagutu, Pogrebnyaya, & Machunda, 2018). Molecular orbital maps were obtained using the VMD plotting program (Qin, Zhu, Liu, Zhang, & Lu, 2012; Zhao, Shan, Yang, Wang, Niu, & Chen, 2015).

#### Statistical analysis

All experiments were conducted in triplicate. The measured data were expressed as mean  $\pm$  standard deviation. Significance between related samples was analyzed according to the one-way ANOVA test at the level of 0.05 ( $p < 0.05$ ) using the SPSS 18.0 (Chicago, IL, USA).

## Results and discussion

### Composition of volatile compounds from oleic acid during heating

As shown in Table 1, a total of 43 volatile compounds, including aldehydes (11), ketones (2), alcohols (5), furans (2), acids (8), esters (12) and alkanes (3) were identified from oleic acid during heating. A heat map was drawn for the volatile compounds obtained from oleic acid during heating to evaluate the variation tendency of compounds at different temperatures. The color of the heat map gradually changes from cold to warm. The cold color represents a low content, and the warm color represents a relatively high content. As shown in Fig. 1(B), the color of most volatile compounds changed gradually from cold to warm with the increase of temperature.

### DFT calculation results of oleic acid oxidation

A total of 30 reactions were obtained by applying DFT to calculate and analyze the chemical reactions during thermal oxidative process of oleic acid, and these 30 reactions were classified and summarized into three reaction pathways, namely, peroxide (ROOH), alkoxy radical (RO•), and peroxide radical (ROO•) pathways (Fig. 2). The molecular structures of the transition states in each pathway were shown in Fig. 3, and the other molecular structures of the reactants, intermediates and final products were shown in Fig. SM1.

### Analysis of the peroxide (ROOH) pathway in the thermal oxidative process of oleic acid

In the initial stage of the oxidation reaction of oleic acid, the hydrogen on the  $\alpha$ -C at the both sites of the carbon-carbon double bond is so reactive that it could easily absorb energy to break, thus form the corresponding alkenyl radical and hydrogen radical (Lu & Chen, 2012; Russell, 1987). Therefore, when oleic acid is thermally oxidized, the hydrogen at C 8 and C 11 positions, which are connected with the C=C double bond, is relatively active to absorb energy, thus causing the C-H bond at C 8 ( $R_1$ ) or C 11 ( $R_2$ ) positions to break, resulting to form the corresponding hydrogen and olefin radicals. The corresponding

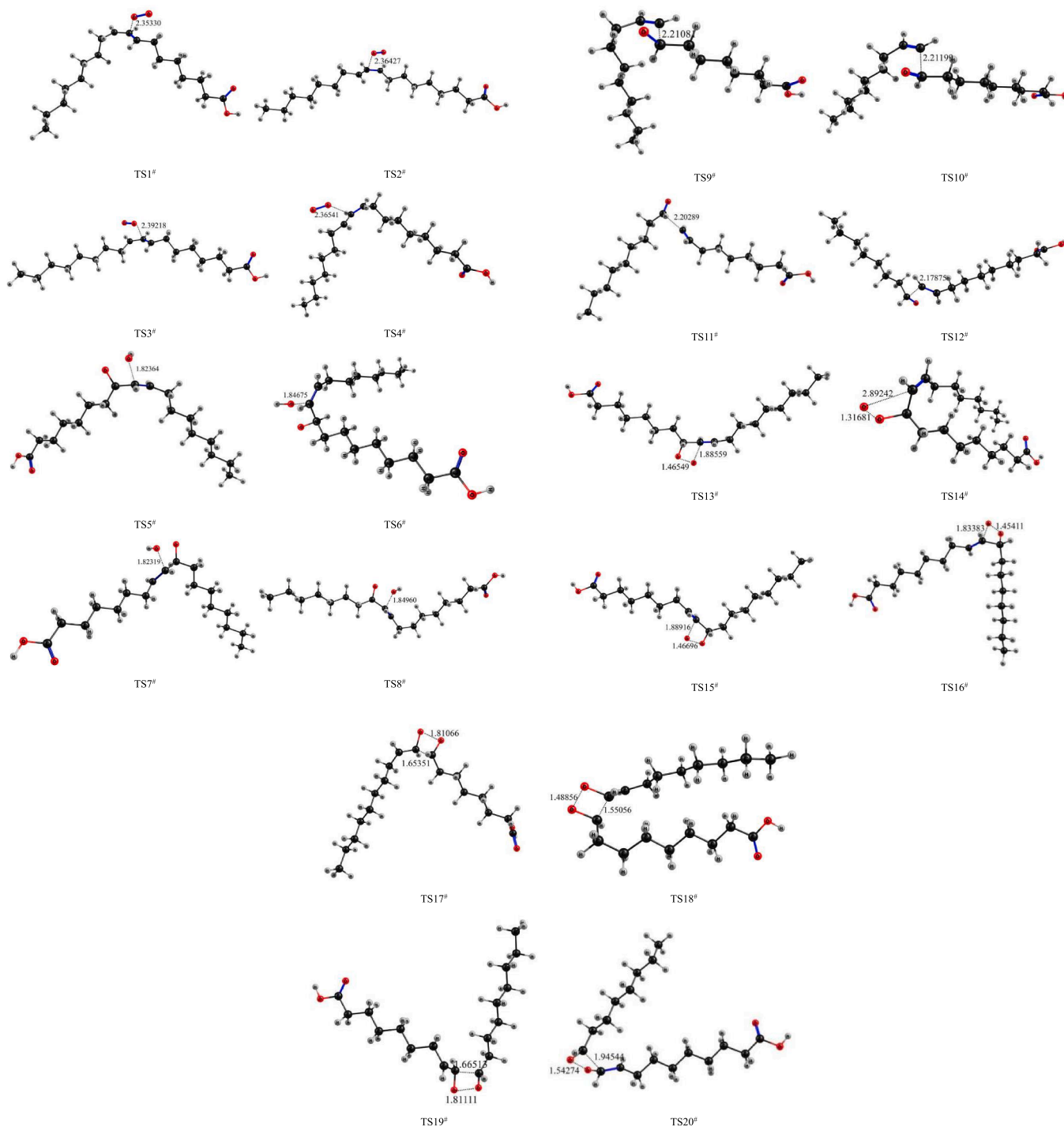


**Fig. 3.** Molecular structure of transition states of oleic acid oxidation reaction. Number of TS1<sup>#</sup>-TS20<sup>#</sup> equal to Fig. 2.

molecular orbital diagrams are shown in Fig. 4A and B, respectively. As shown in Fig. 4, the darker the color, the denser the electron cloud, and the easier the reaction would be.

Next, the olefin radical at the C 8 position can form a conjugate system with carbon-carbon double bonds at the C 8, C 9, and C 10 positions with  $\pi$  bonds. The olefin radical at the C 11 position can also form a conjugate system with carbon-carbon double bonds at the C 9, C 10, and C 11 positions with  $\pi$  bonds. Given the energy instability of this conjugated system, the rearrangement of the carbon-carbon double bond and radicals are observed. The conjugated system at C 8, C 9, and C 10 positions can rearrange into olefin radicals with  $C_9=C_{10}$  or  $C_8=C_9$ . As

shown in Fig. 5(A-a), the C 8, C 9, and C 10 conjugated system has high charge density, which is vulnerable to be attacked. The oxygen reacts with the rearranged olefin radical then form the peroxide radical 8-ROO• or 10-ROO• respectively via transition state (TS1<sup>#</sup> or TS3<sup>#</sup>). While the C 9, C 10, and C 11 position conjugated systems rearrange into  $C_{10}=C_{11}$  or  $C_9=C_{10}$  olefin radicals, as shown in Fig. 5(A-b). After the oxygen reacts via the transition state TS2<sup>#</sup> or TS4<sup>#</sup>, peroxide radicals 9-ROO• or 11-ROO• are formed.

8-ROO•, 9-ROO•, 10-ROO•, and 11-ROO• can then recombine with the hydrogen radicals shed by oleic acid or take over the H atoms of other C-H bonds to form 8-ROOH, 9-ROOH, 10-ROOH, and 11-ROOH.

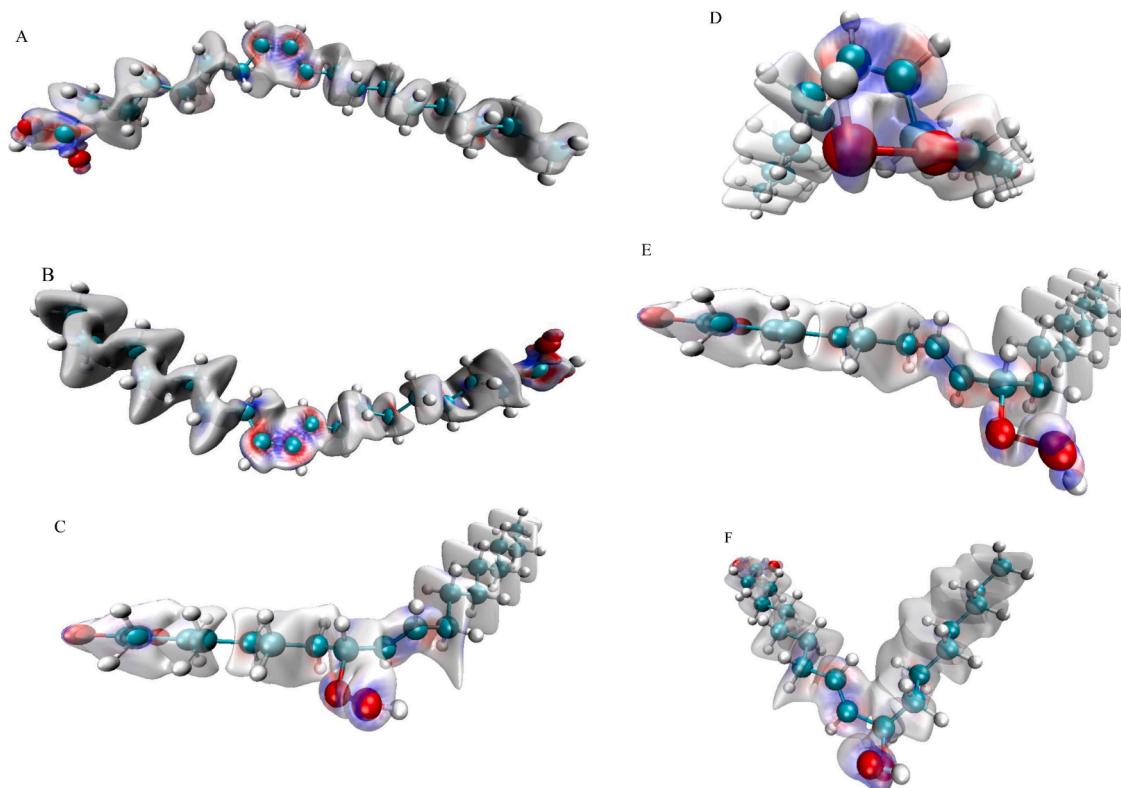


Fig. 4. Molecular orbital diagram. (A): 8-R•;(B): 11-R•; (C): 8-ROOH;(D): 9-ROOH; (E): 10-ROOH; (F): 11-ROOH.

These peroxides are unstable and will further oxidize. As shown in Fig. 5 (A-a), the hydroxyl group in the peroxy group of 8-ROOH will attack adjacent carbon atoms C 7 or C 9, and the specific position is known from the molecular orbital diagram. As shown in Fig. 4 (C), the electron cloud density on the C 9 side is higher than that on the C 7 side. Thus, the hydroxyl group in the peroxy hydroxyl group of 8-ROOH will attack C 9. Similarly, as shown in path b, c, d in Fig. 5A and D, E, F in Fig. 4, the hydroxyl group in the peroxy hydroxyl group of 9-ROOH, 10-ROOH or 11-ROOH will attack C 10, C 9, C 10, respectively. At this point, the corresponding structures of the transition states are TS5<sup>#</sup>, TS6<sup>#</sup>, TS7<sup>#</sup>, and TS8<sup>#</sup>, then decanal, CHO(CH<sub>2</sub>)<sub>6</sub>COOH, nonanal, CHO(CH<sub>2</sub>)<sub>7</sub>COOH, octanal, and CHO(CH<sub>2</sub>)<sub>8</sub>COO are formed, which ultimately constitute the peroxide (ROOH) pathways (Path1-4). The final products after decomposition of the above peroxides are as following: 8-ROOH cleaves to produce decanal and 7-oxo-octanoic acid; 9-ROOH cleaves to produce nonanal and CHO(CH<sub>2</sub>)<sub>7</sub>COOH; 10-ROOH cleaves to produce the same products as 9-ROOH; 11-ROOH cleaves to produce octanal and CHO(CH<sub>2</sub>)<sub>8</sub>COOH.

#### Analysis of the alkoxy radical (RO•) pathway in the thermal oxidative process of oleic acid

During heating, the O—O bonds in the peroxy hydroxyl groups of peroxides 8-ROOH, 9-ROOH, 10-ROOH, and 11-ROOH could also absorb energy leading to the breakage of O—O bonds to remove the active hydroxyl radicals (•OH), which generates different reaction intermediates 8-RO•, 9-RO•, 10-RO•, and 11-RO•. These alkoxy radicals would attack the adjacent C atom, which causes oxidative breakage of the adjacent C—C bond. As shown in Fig. 5(B-a), 8-RO• could attack C 7 or C 9. Meanwhile, it can be seen from Fig. SM2(A) that the electron cloud density on the C 9 side is higher than that on the C 7 side. Thus, 8-RO• would predominantly attack C 9. In the same way, 9-RO• would predominantly attack C 10 (Fig. 5(B-b)); 10-RO• would predominantly attack C 9 (Fig. 5(B-c)); 11-RO• would predominantly attack C 10 (Fig. 5

(B-d)). And the corresponding molecular orbital diagrams are shown in Fig. SM2B, C and D, respectively. The above mentioned substances via transition state structures (TS9<sup>#</sup>, TS10<sup>#</sup>, TS11<sup>#</sup>, and TS12<sup>#</sup>) form final products, such as CHO(CH<sub>2</sub>)<sub>6</sub>COOH, nonanal, CHO(CH<sub>2</sub>)<sub>7</sub>COOH, octanal and four olefin radicals, which constitute the alkoxy radical (RO•) pathways (Path 5–8). The final oxidation products of the alkoxy radicals pathways are as following: 8-RO• produces compound CHO(CH<sub>2</sub>)<sub>6</sub>COOH and CH<sub>3</sub>(CH<sub>2</sub>)<sub>7</sub>CH=CH; 9-RO• produces compound CHO(CH<sub>2</sub>)<sub>7</sub>COOH and CH<sub>3</sub>(CH<sub>2</sub>)<sub>6</sub>CH=CH; 10-RO• produces compound nonanal and COOH(CH<sub>2</sub>)<sub>6</sub>CH=CH; 11-RO• produces compound octanal and COOH(CH<sub>2</sub>)<sub>7</sub>CH=CH.

#### Analysis of the peroxide radical (ROO•) pathway in the thermal oxidative process of oleic acid

The peroxide radical (ROO•) structure is an extreme oxidizing agent, and the O—O• would attack the adjacent C atom, which cause oxidative breakage of the adjacent C—C bond. As shown in Fig. 5(C-a), 8-ROO• would attack C 7 or C 9. The molecular orbital shows that the electron cloud density on the C 9 side is higher than that on the C 7 side (Fig. SM2 [E]). As a result, the main attacking side is C 9. Similarly, as shown b, c, d in Fig. 5C and F, G, H in Fig. SM2, the O• of 9-ROO•, 10-ROO• or 11-ROO• would primarily attack C 10, C 9, C 10, respectively. The corresponding processes lead to the formation of transition state (TS13<sup>#</sup>, TS14<sup>#</sup>, TS15<sup>#</sup>, and TS16<sup>#</sup>) and three intermediate products (CH<sub>3</sub>(CH<sub>2</sub>)<sub>8</sub>(CHO•)<sub>2</sub>(CH<sub>2</sub>)<sub>6</sub>COOH, CH<sub>3</sub>(CH<sub>2</sub>)<sub>7</sub>(CHO•)<sub>2</sub>(CH<sub>2</sub>)<sub>7</sub>COOH, CH<sub>3</sub>(CH<sub>2</sub>)<sub>6</sub>(CHO•)<sub>2</sub>(CH<sub>2</sub>)<sub>8</sub>COOH). Then the C—C bonds absorb energy to break between the two alkoxy radicals via transition state (TS17<sup>#</sup>, TS18<sup>#</sup>, TS19<sup>#</sup>, and TS20<sup>#</sup>). The final oxidation products of the above peroxide radicals are as followed: 8-ROO• cleavage produces compound CHO(CH<sub>2</sub>)<sub>6</sub>COOH and CH<sub>3</sub>(CH<sub>2</sub>)<sub>8</sub>CHO•; 9-ROO• cleavage produces compound CHO(CH<sub>2</sub>)<sub>7</sub>COOH and CH<sub>3</sub>(CH<sub>2</sub>)<sub>7</sub>CHO•; 10-ROO• cleavage produces compound CHO(CH<sub>2</sub>)<sub>7</sub>COOH and CH<sub>3</sub>(CH<sub>2</sub>)<sub>7</sub>CHO•; 11-ROO• cleavage produces compound CHO(CH<sub>2</sub>)<sub>8</sub>COOH and CH<sub>3</sub>(CH<sub>2</sub>)<sub>6</sub>CHO•.

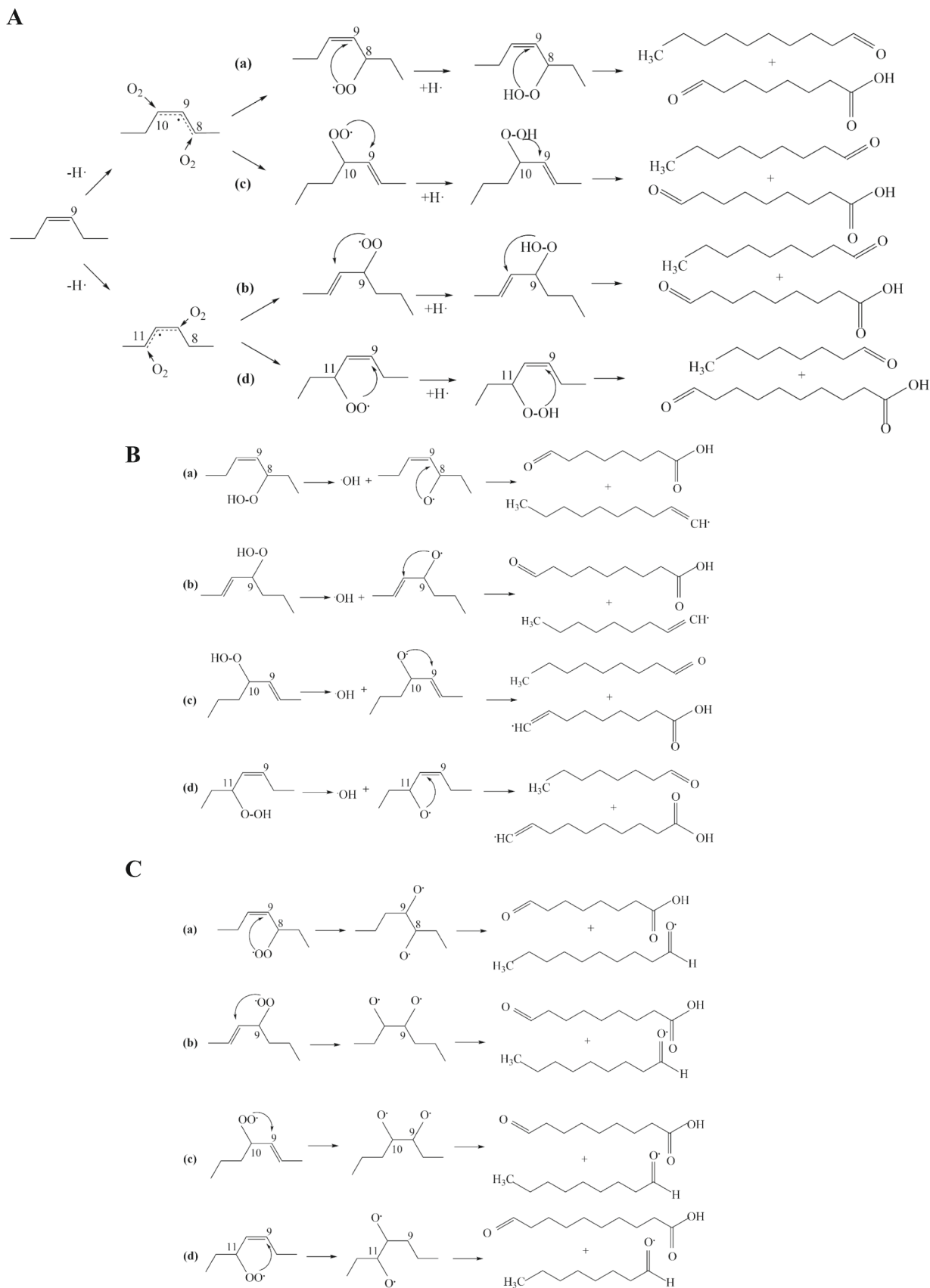
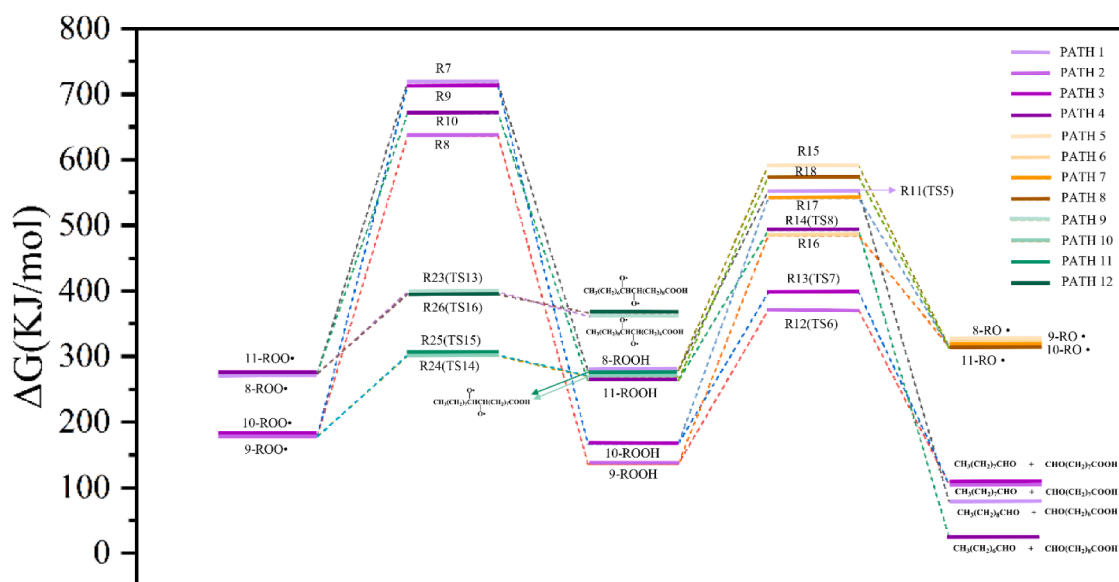


Fig. 5. Potential decomposition pathway of oleic acid thermal oxidation. (A) peroxide (ROOH) pathway; (B) alkoxy radical (RO•) pathway; (C) peroxide radical (ROO•) pathway.

A



B

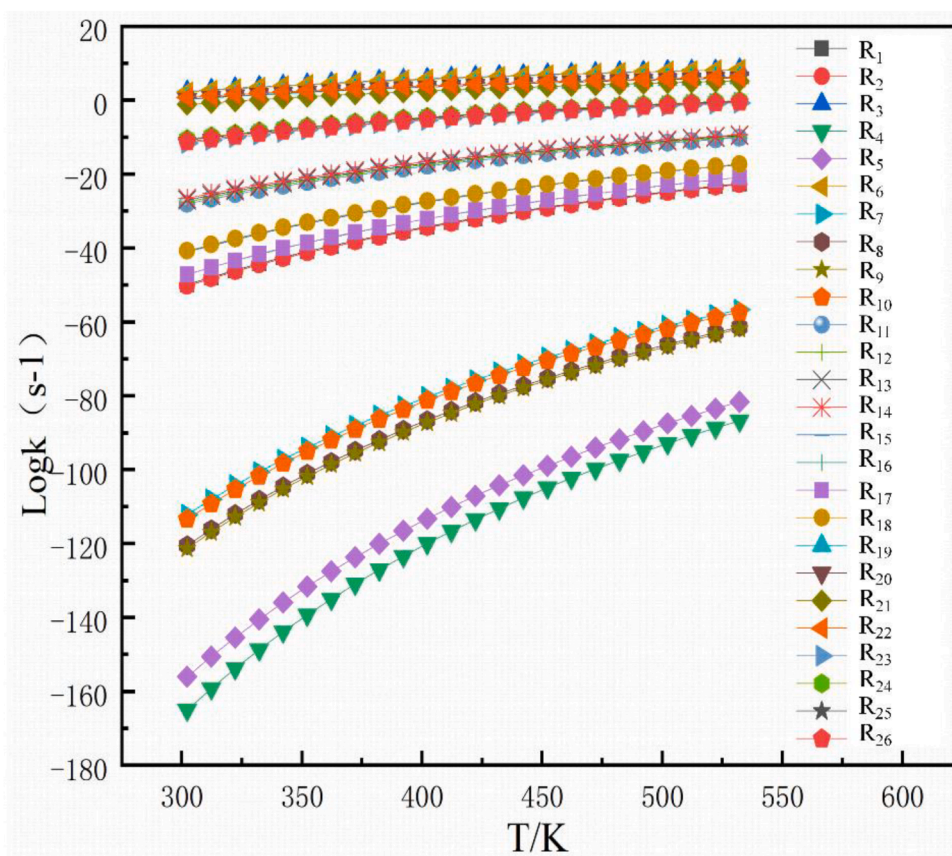


Fig. 6. Potential energy diagram and rate constants of oleic acid oxidation reaction. (A): Energy surfaces of key reactions of oleic acid thermal oxidation; (B): Reaction rate constants of oleic acid thermal oxidation process.

### Determination of key reactions and reaction priority of different reaction pathways in oleic acid thermal oxidation process

As shown in Fig. 2, in the initial stage of oleic acid oxidation, peroxide (ROOH), alkoxy radical (RO•) and peroxide radical (ROO•) pathways go through the dehydrogenation of  $\alpha$ -C (R<sub>1</sub>-R<sub>2</sub>) and the subsequent combination reactions with oxygen (R<sub>3</sub>-R<sub>6</sub>) together. And the energy required for hydrocarbon bond dissociation at the C 8 and C 11 positions of oleic acid are 362.77 KJ/mol (R<sub>1</sub>) and 364.82 KJ/mol (R<sub>2</sub>), respectively, which are basically the same (Fig. SM3). Fig. 6A shows the energy barriers of key reactions of oleic acid thermal oxidation. And the energy barriers of all reactions in the oleic acid thermal oxidation process are shown in Fig. SM3. As shown in Fig. SM3, the energy requirements of R<sub>3</sub> and R<sub>6</sub> are 363.88 and 364.16 KJ/mol with C8 or C11 as main reaction sites respectively in the following reaction. Meanwhile, with C9 or C10 as main reaction sites, the energy requirements of R<sub>4</sub> and R<sub>5</sub> are 1330.77 KJ/mol (R<sub>4</sub>) and 1280.27 KJ/mol (R<sub>5</sub>), respectively. It is obvious that R<sub>4</sub> and R<sub>5</sub> require much more energy than R<sub>3</sub> and R<sub>6</sub>, also indicates that R<sub>3</sub> and R<sub>6</sub> are the major reactions at lower temperatures, while R<sub>4</sub> and R<sub>5</sub> only react at higher temperatures. Additionally, the product of C8 and C11 are more easily produced than that of C9 and C10, which is the same as the results of Frankel (Frankel, 1980).

It is generally believed that the branch chemical reaction is the key reaction in the reaction pathway. Therefore, the following reactions R<sub>7</sub>-R<sub>10</sub> are considered as the key reaction of peroxide (ROOH) and alkoxy radical (RO•) pathway, and reactions (R<sub>23</sub>-R<sub>26</sub>) are the key reaction of peroxide radical (ROO•) pathways. Meanwhile, as shown in Fig. 6A, the energy requirements for reactions (R<sub>7</sub>-R<sub>10</sub>) are much higher than that of reactions (R<sub>23</sub>-R<sub>26</sub>). Fig. 6B shows that the rate constants of reactions (R<sub>7</sub>-R<sub>10</sub>) are also lower than those of reactions (R<sub>23</sub>-R<sub>26</sub>). This means that the peroxide radical (ROO•) pathway occurs in preference to the peroxide (ROOH) and alkoxy radical (RO•) pathway. In the following chemical reaction pathway, 8-ROOH, 9-ROOH, 10-ROOH and 11-ROOH are located at the branching points of the reaction pathway. Therefore, the chemical reactions with these compounds as reactants are the key reactions of the reaction pathway. Specifically, reactions (R<sub>11</sub>-R<sub>14</sub>) are the key reaction of the peroxides (ROOH) pathway, and reactions (R<sub>15</sub>-R<sub>18</sub>) are the key reaction of the alkoxy radical (RO•) pathway. Meanwhile, as shown in Fig. 6A, the energy requirements for reactions (R<sub>15</sub>-R<sub>18</sub>) are much higher than that of reactions (R<sub>11</sub>-R<sub>14</sub>). Fig. 6B shows that the rate constants of reactions (R<sub>15</sub>-R<sub>18</sub>) are also lower than those of reactions (R<sub>11</sub>-R<sub>14</sub>). This means that the peroxide (ROOH) pathway occurs in preference to the alkoxy radical (RO•) pathway.

From the results discussed above, as shown in Fig. SM3, it can be inferred that R<sub>4</sub> and R<sub>5</sub> require much more energy than R<sub>3</sub> and R<sub>6</sub> and that the concentrations of the final products of Path 1, 4, 5, 8, 9, 12 are higher than those of Path 2, 3, 6, 7, 10, 11. This means that the concentration of decanal, CHO(CH<sub>2</sub>)<sub>6</sub>COOH, octanal and CHO(CH<sub>2</sub>)<sub>8</sub>COOH is higher than that of nonanal and CHO(CH<sub>2</sub>)<sub>7</sub>COOH. However, compounds such as CHO(CH<sub>2</sub>)<sub>6</sub>COOH, CHO(CH<sub>2</sub>)<sub>7</sub>COOH and CHO(CH<sub>2</sub>)<sub>8</sub>COOH is not discussed in this paper due to their lower volatility. Besides, Path 1 is the main production pathway for decanal, and Path 4 is the main production pathway for octanal. As shown in Fig. 6B, the reaction rate constants of R<sub>7</sub> and R<sub>10</sub>, R<sub>11</sub> and R<sub>14</sub> are basically the same. However, as shown in Fig. 6A, the energy barrier of TS<sub>5</sub><sup>#</sup> is slightly higher than that of TS<sub>8</sub><sup>#</sup>. Therefore, the theoretical deduction of the obtained compound content is octanal > decanal > nonanal. However, as shown in Tab. 1, the actual compound content at each temperature is nonanal > octanal > decanal. The reason is that in our previous researches we found that among the saturated aldehydes below ten carbons, only decanal can continue to oxidize and decompose to aldehydes with lower carbon chains during heating, and that nonanal is the major product (Gao, Bao, Wang, et al., 2023).

Meanwhile, it is also founded that the oxidation products from the C8 and C11 positions are compounds with a carbon chain of 8 carbons, such as octane, octanal and octanoic acid based on experimental data.

Moreover, the final products of peroxide radical pathway could be formed at a lower temperature and have a relatively high content, such as octane, heptanal and undecanal. Meanwhile, the oxidation products from the C9 and C10 positions are compounds with a carbon chain of 9 carbons, such as nonanal and nonanoic acid. It is also founded that 8 carbon chain compounds are produced at relatively lower temperatures than 9-carbon compounds, while the content is higher. These results are basically consistent with the calculations. In summary, during oleic acid thermal oxidation, the priority order in which the reaction pathways occur is that the peroxide radical pathway had priority over the peroxide pathway, which then had priority over the alkoxy radical pathway.

## Conclusion

The application of DFT to the field of food flavor chemistry can effectively reveal the mechanism of volatile flavor substance formation during food thermal processing. During oleic acid thermal oxidation, a total of 30 reactions were obtained by applying DFT calculation, and these 30 reactions were classified and summarized into three reaction pathways, namely, peroxide, alkoxy radical, and peroxide radical pathways. The priority order of these reaction pathways occurred is that the peroxide radical pathway had priority over the peroxide pathway, which then had priority over the alkoxy radical pathway.

## CRedit authorship contribution statement

**Lin Xiao:** Data curation, Writing – original draft, Software. **Shang Wang:** Visualization, Investigation. **Yi Wang:** Software. **Binchen Wang:** Software. **Chaofan Ji:** . **Xinping Lin:** Data curation. **Huipeng Liang:** Software. **Sufang Zhang:** Supervision. **Xianbing Xu:** Formal analysis. **Liang Dong:** Conceptualization, Methodology.

## Declaration of Competing Interest

The authors declare that they have no known competing financial interests or personal relationships that could have appeared to influence the work reported in this paper.

## Data availability

The authors do not have permission to share data.

## Acknowledgements

We thank the support of National Natural Science Foundation of China (No. 31871760).

## Appendix A. Supplementary data

Supplementary data to this article can be found online at <https://doi.org/10.1016/j.fochx.2023.100737>.

## References

- Bao, Y. X., Du, J., Xu, C., Wang, M. T., Wang, B. C., Xiao, L., ... Dong, L. (2022). Detailed temperature-dependent study of linoleic acid oxidative decomposition into volatile compounds in the heating process. *Journal of Food Processing and Preservation*, 46(4), Article e16445.
- Benkhoud, H., Rabet, Y. M., Gara Ali, M., Mezni, M., & Hosni, K. (2022). Essential oils as flavoring and preservative agents: Impact on volatile profile, sensory attributes, and the oxidative stability of flavored extra virgin olive oil. *Journal of Food Processing and Preservation*, 46(5), e15379.
- Chai, D., Li, C. W., Zhang, X. X., Yang, J. F., Liu, L. Z., Xu, X. B., ... Dong, L. (2019). Analysis of volatile compounds from wheat flour in the heating process. *International Journal of Food Engineering*, 15(10). <https://doi.org/10.1515/ijfe-2019-20252>
- Cheng, H., Chen, J. L., Li, X., Pan, J. X., Xue, S., Liu, D. H., & Ye, X. Q. (2015). Differentiation of the volatile profiles of Chinese bayberry cultivars during storage by HS-SPME GC/MS combined with principal component analysis. *Postharvest Biology and Technology*, 100, 59–72.

- Chen, Y., Li, W. Q., Yu, Y. S., Wang, M. N., Blank, I., Zhang, Y., & Liu, Y. (2023). Elucidation of the impact of steaming on the key odorants of jinhua dry-cured ham using the sensomics approach. *Journal of Agricultural and Food Chemistry*, *71*, 4932–4942.
- Elqahatani, Z. M., Aman, S., Mehmood, S., Ali, Z., Hussanan, A., Ahmad, N., ... Farid, H. M. T. (2022). n-Type narrow band gap A(3)InAs(3) (A = Sr and Eu) Zintl phase semiconductors for optoelectronic and thermoelectric applications. *Journal of Taibah University for Science*, *16*(1), 660–669.
- Elroby, S. A., Banaser, B. A., Aziz, S. G., Jedidi, A., Hassan, W. I., & Osman, O. I. (2022). Zn<sup>2+</sup>-Schiff's base complex as an "On-Off-On" molecular switch and a fluorescence probe for Cu<sup>2+</sup> and Ag<sup>+</sup> ions. *Journal of Fluorescence*, *32*(2), 691–705.
- Endo, Y., Sakamoto, Y., Kajii, Y., & Enami, S. (2022). Decomposition of multifunctionalized alpha-alkoxyalkyl-hydroperoxides derived from the reactions of Criegee intermediates with diols in liquid phases. *Physical Chemistry Chemical Physics*, *24*(19), 11562–11572.
- Frankel, E. N. (1980). Lipid oxidation. *Progress in Lipid Research*, *19*(1–2), 1–22.
- Frankel, E. N. (1984). Chemistry of free-radical and singlet oxidation of lipids. *Progress in Lipid Research*, *23*(4), 197–221.
- Russell, G. A. (1987). Free radical chain processes in aliphatic systems involving an electron transfer reaction. *Advances in Physical Organic Chemistry*, *23*, 271–322.
- Friedrich, B. (2016). How did the tree of knowledge get its blossom? The rise of physical and theoretical chemistry, with an eye on Berlin and Leipzig. *Angewandte Chemie-International Edition*, *55*(18), 5378–5392.
- Gao, P. X., Bao, Y. X., Wang, S., Lei, L. M., Wang, B. C., Xiao, L., ... Dong, L. (2023). Mechanism of palmitoleic acid oxidation into volatile compounds during heating. *Flavour and Fragrance Journal*, *38*(2), 95–107.
- González, J., Giménez, X., & Bofill, J. M. (2002). A reaction path Hamiltonian defined on a Newton path. *Journal of Chemical Physics*, *116*(20), 8713–8722.
- Huang, X. H., Zheng, X., Chen, Z. H., Zhang, Y. Y., Du, M., Dong, X. P., ... Zhu, B. W. (2019). Fresh and grilled eel volatile fingerprinting by e-Nose, GC-O, GC-MS and GC×GC-QTOF combined with purge and trap and solvent-assisted flavor evaporation. *Food Research International*, *115*, 32–43.
- Kvasnyuk, E., Sysa, A., Al Saud, S., Shahab, S., Sheikhi, M., Kaviani, S., & Zinchenko, A. (2023). Quantum chemical modeling, synthesis, spectroscopic (FT-IR, excited states, UV/VIS) studies, FMO, QAIM, ELF, LOL, NBO, NLO and QSAR analyses of nelarabine. *Biointerface Research in Applied Chemistry*, *13*(2), 1–35.
- Li, G. X., Luo, Z. Y., Wang, W. B., & Cen, J. M. (2020). A study of the mechanisms of guaiacol pyrolysis based on free radicals detection technology. *Catalysts*, *10*(3), 295–303.
- Liu, X. F., Wang, S., Tamogami, S., Chen, J. Y., & Zhang, H. (2021). Volatile profile and flavor characteristics of ten edible oils. *Analytical Letters*, *54*(9), 1423–1438.
- Liu, Y. P., Li, Q. R., Yang, W. X., Sun, B. G., Zhou, Y., Zheng, Y., ... Yang, W. J. (2020). Characterization of the potent odorants in *Zanthoxylum armatum* DC Prodr. Pericarp oil by application of gas chromatography-mass spectrometry-olfactometry and odor activity value. *Food Chemistry*, *319*, 126564.
- Lu, T., & Chen, F. W. (2012). Multiwfn: A multifunctional wavefunction analyzer. *Journal of Computational Chemistry*, *33*(5), 580–592.
- Mahmoud, M. A. M., Shiroudi, A., Abdel-Rahman, M. A., Shibl, M. F., Abdel-Azeim, S., & El-Nahas, A. M. (2021). Structures, energetics, and kinetics of H-atom abstraction from methyl propionate by molecular oxygen: Ab initio and DFT investigations. *Computational and Theoretical Chemistry*, *1196*, 113119.
- Matheis, K., & Granvogel, M. (2019). Unraveling of the fishy off-flavor in steam-treated rapeseed oil using the sensomics concept. *Journal of Agricultural and Food Chemistry*, *67*(5), 1484–1494.
- Müller, C. S. L., Shabani, M., Wagenpfeil, G., & Vogt, T. (2021). Granuloma anulare, Necrobiosis lipoidica und deren Assoziation zu Adipositas, Diabetes mellitus und hämatologischen Malignomen. *Aktuelle Dermatologie*, *47*(04), 159–161.
- Otero, L., Ramos, A. M., de Elvira, C., & Sanz, P. D. (2007). A model to design high-pressure processes towards a uniform temperature distribution. *Journal of Food Engineering*, *78*(4), 1463–1470.
- Pedersen, J., & Mikkelsen, K. V. (2022). A benchmark study of aromaticity indexes for benzene, pyridine and the diazines – I. Ground state aromaticity. *Rsc Advances*, *12*(5), 2830–2842.
- Qin, M. Y., Zhu, X. S., Liu, K. L., Zhang, Q. B., & Lu, P. X. (2012). Imprints of the molecular-orbital geometry on the high-harmonic ellipticity. *Optics Express*, *20*(18), 20181–20190.
- Raghavachari, K., Trucks, G. W., Pople, J. A., & Head-Gordon, M. (1989). A fifth-order perturbation comparison of electron correlation theories. *Chemical Physics Letters*, *157*(6), 479–483.
- Raos, N. (2021). The clash of old and new chemistry in Croatia. *Journal of Chemists and Chemical Engineers*, *70*(3–4), 163–170.
- Ryu, H., Park, J., Kim, H. K., Park, J. Y., Kim, S.-T., & Baik, M.-H. (2018). Pitfalls in computational modeling of chemical reactions and how to avoid them. *Organometallics*, *37*(19), 3228–3239.
- Shabani, M., Latina, J., Li, Z., Sesso, J., Kapoor, K., Demehri, S., ... Zadeh, A. (2020). Comparison of ultra-high-resolution with conventional CT-derived coronary lumen visibility in patients with coronary artery disease. *Journal of Cardiovascular Computed Tomography*, *14*(3), S41.
- Turovskiy, M. A., Raksha, O. V., Opeida, I. O., Turovska, M. O., & Zaikov, G. E. (2007). Molecular modelling of aralkyl hydroperoxides homolysis. *Oxidation Communications*, *30*(3), 504–512.
- Wagutu, A. W., Pogrebnaya, T., & Machunda, R. (2018). Study of interaction of chitosan with Fluoride. *Biointerface Research in Applied Chemistry*, *8*(3), 3170–3177.
- Wang, B. C., Xiao, L., Chai, D., Jiang, Y. M., Wang, M. T., Xu, X. B., ... Dong, L. (2020). Metabolite analysis of wheat dough fermentation incorporated with buckwheat. *Food Science & Nutrition*, *8*(8), 4242–4251.
- Wang, H. X., Qin, L., Wang, Y., Zhou, D. Y., Song, S., Wang, X. S., & Zhu, B. W. (2014). Effects of heating conditions on fatty acids and volatile compounds in foot muscle of abalone *Haliotis discus hannai* Ino. *Fisheries Science*, *80*, 1097–1107.
- Xiao, L., Li, C. W., Chai, D., Chen, Y., Wang, Z. Y., Xu, X. B., ... Dong, L. (2020). Volatile compound profiling from soybean oil in the heating process. *Food Science & Nutrition*, *8*(2), 1139–1149.
- Xie, Q. S., Xu, B. C., Xu, Y., Yao, Z., Zhu, B. W., Li, X. F., & Sun, Y. (2022). Effects of different thermal treatment temperatures on volatile flavour compounds of water-boiled salted duck after packaging. *LWT-Food Science and Technology*, *154*, Article 112625.
- Zhao, M. F., Shan, X., Yang, J., Wang, E. L., Niu, S. S., & Chen, X. J. (2015). Observation of interference effects in (e, 2e) electron momentum spectroscopy of SF<sub>6</sub>. *Chinese Journal of Chemical Physics*, *28*(5), 539–544.
- Zhao, W., Yang, R. J., Shi, X. Q., Pan, K., Zhang, S., Zhang, W. B., & Hua, X. (2011). Oxidation of oleic acid under pulsed electric field processing. *Food Research International*, *44*(5), 1463–1467.
- Zhou, Q., Liu, S. M., Liu, Y., & Song, H. L. (2019). Comparative analysis of volatiles of 15 Brands of extra-virgin olive oils using solid-phase microextraction and solvent-assisted flavor evaporation. *Molecules*, *24*(8), 1512–1530.